AFRL-SN-RS-TR-1998-215
In-House Report
March 1999

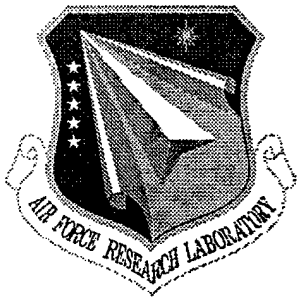

OPERATING THE CROSS SPECTRAL METRIC ALGORITHM WITH LIMITED SECONDARY DATA SUPPORT

Todd B. Hale, Capt., USAF

AIR FORCE RESEARCH LABORATORY
SENSORS DIRECTORATE
ROME RESEARCH SITE
ROME, NEW YORK

Although this report references a limited document (*), listed on page 24, no limited information has been extracted.

This report has been reviewed by the Air Force Research Laboratory, Information Directorate, Public Affairs Office (IFOIPA) and is releasable to the National Technical Information Service (NTIS). At NTIS it will be releasable to the general public, including foreign nations.

AFRL-SN-RS-TR-1998-215 has been reviewed and is approved for publication.

APPROVED:

GERARD J. GENELLO
Chief, Radar Signal Processing Branch
Sensors Directorate

FOR THE DIRECTOR:

ROBERT G. POLCE, Acting Chief
Rome Operations Office
Sensors Directorate

If your address has changed or if you wish to be removed from the Air Force Research Laboratory Rome Research Site mailing list, or if the addressee is no longer employed by your organization, please notify AFRL/SNRT, 26 Electronic Parkway, Rome, NY 13441-4514. This will assist us in maintaining a current mailing list.

Do not return copies of this report unless contractual obligations or notices on a specific document require that it be returned.

REPORT DOCUMENTATION PAGE	Form Approved OMB No. 0704-0188

1. AGENCY USE ONLY *(Leave blank)*	2. REPORT DATE	3. REPORT TYPE AND DATES COVERED
	March 1999	In-House, Jan 98 - Jun 98

4. TITLE AND SUBTITLE

OPERATING THE CROSS SPECTRAL METRIC ALGORITHM WITH LIMITED SECONDARY DATA SUPPORT

5. FUNDING NUMBERS

PE - 62702F
PR - 4506
TA - SN
WU- OT

6. AUTHOR(S)

Todd B. Hale, Capt., USAF

7. PERFORMING ORGANIZATION NAME(S) AND ADDRESS(ES)

Air Force Research Laboratory/SNRT
26 Electronic Parkway
Rome, NY 13441-4514

8. PERFORMING ORGANIZATION REPORT NUMBER

AFRL-SN-RS-TR-1998-215

9. SPONSORING/MONITORING AGENCY NAME(S) AND ADDRESS(ES)

Air Force Research Laboratory/SNRT
26 Electronic Parkway
Rome, NY 13441-4514

10. SPONSORING/MONITORING AGENCY REPORT NUMBER

AFRL-SN-RS-TR-1998-215

11. SUPPLEMENTARY NOTES

Air Force Research Laboratory Project Engineer: Capt. Todd B. Hale/SNRT/(315) 330-1896

12a. DISTRIBUTION AVAILABILITY STATEMENT

APPROVED FOR PUBLIC RELEASE; DISTRIBUTION UNLIMITED.

12b. DISTRIBUTION CODE

13. ABSTRACT *(Maximum 200 words)*

One of the primary problems with the application of Space-Time Adaptive Processing (STAP) techniques is secondary data support for the covariance matrix estimate. Reed has shown the required secondary data support to achieve performance within 3 db of optimal SINR is approximately twice the Degrees Of Freedom (DOF) used. Reed proved this rule for Sample Matrix Inversion (SMI) techniques. A newer class of reduced dimension STAP algorithms uses a decomposition of the sample covariance matrix, thereby deviating from the SMI algorithm class. This report focuses on the performance of the Cross Spectral Metric (CSM) Algorithm with varying secondary data support sizes. The algorithm is shown to be highly susceptible to poor estimation of eigenvalues in the noise subspace. This susceptibility is manifested through large drops in output SINR with secondary data set sizes near the space-time product. To determine the cause of these performance drops, the CSM algorithm is recast in the structure of the eigenbeam model for SMI techniques presented by Gabriel. This new form of the CSM weight vector illustrates that eigenvalue spread in the noise subspace, a result of insufficient sample support, has a direct negative impact on the overall weight vector. Furthermore, eigenvalue spread is mitigated through the use of a diagonally loaded sample covariance matrix. Reducing the eigenvalue spread reduces the impact of cross spectral eigenbeams lying in the noise subspace. Monte Carlo simulations show the SINR performance drop mentioned previously is alleviated through the use of an appropriate diagonal load factor.

14. SUBJECT TERMS	15. NUMBER OF PAGES
adaptive processing, signal processing, cross spectral metric, secondary data, covariance matrix	36
	16. PRICE CODE

17. SECURITY CLASSIFICATION OF REPORT	18. SECURITY CLASSIFICATION OF THIS PAGE	19. SECURITY CLASSIFICATION OF ABSTRACT	20. LIMITATION OF ABSTRACT
UNCLASSIFIED	UNCLASSIFIED	UNCLASSIFIED	UL

Table of Contents

1.0 INTRODUCTION 1

1.1 Notation 2

1.2 Report Overview 2

2.0 THE CSM ALGORITHM 3

2.1 Covariance Matrix Estimation 5

2.2 Generating Data for Performance Analysis 6

3.0 SAMPLE SUPPORT AND THE CSM ALGORITHM 7

3.1 Simulation Procedures 7

3.2 Simulation Results 7

4.0 PERFORMANCE ANALYSIS 11

4.1 Covariance Matrix Estimation Error 11

4.2 Relationship of Estimation Error and CSM 13

4.3 Diagonal Loading 15

5.0 CONCLUSIONS 20

List of Figures

1 CSM Algorithm Block Diagram. 4
2 CSM and corresponding eigenvalue magnitudes for scenario 1 using known covariance. 8
3 Optimum SINR Curve Versus N_{DOF} for scenario 1. 8
4 CSM and corresponding eigenvalue magnitudes for scenario 2 using known covariance. 9
5 Optimum SINR curve versus N_{DOF} for scenario 2. 9
6 Overlay Of SINR Curves For $N_{\mathrm{DOF}} \leq 65$ For Scenario 1. 10
7 Overlay Of SINR Curves For $N_{\mathrm{DOF}} \geq 65$ For Scenario 1. 10
8 Overlay Of SINR for scenario 2. 10
9 Eigenstructure of the known covariance matrix used for the eigenbeam analysis. 13
10 Eigenvalue spread in the noise subspace with MN secondary data vectors, single realization. 13
11 Eigenvalue spread in the noise subspace with $2MN$ secondary data vectors, single realization. 14
12 Eigenvalue spread in the noise subspace with $6MN$ secondary data vectors, single realization. 14
13 Relationship of the scale factor in Eqn. (18) to sample support for eigenbeams occupying the noise subspace for the eigenbeam analysis example. 16
14 Relationship of the scale factor in Eqn. (18) to sample support for eigenbeams occupying the noise subspace when using diagonal loading. 16
15 Impact of diagonal loading the covariance matrix estimate on CSM algorithm performance with small data set sizes for scenario 2. 19
16 The subspace structure for scenario 3 shown with eigenvalues. 19
17 Impact of diagonal loading the covariance matrix estimate on CSM algorithm performance. . 19

List of Tables

1 Parameters for scenario 1. 21

2 Parameters for scenario 2. 22

3 Parameters for scenario 3. 23

1.0 INTRODUCTION

Space-Time Adaptive Processing (STAP) algorithms have been the subject of intense interest for several years. This interest occurs primarily because the algorithms offer significant improvement in target detection capability for an array antenna in the presence of strong interference. The auto correlation of the interference environment allows the algorithm to accurately estimate and reject the interference, thereby enhancing the desired signal.

The strength of STAP is found through incorporation of the interference estimate. However, it is also one of the biggest drawbacks in terms of practical application. Reed [1] has shown the sample support required to estimate the interference covariance matrix for Sample Matrix Inversion (SMI) techniques is approximately two times the Degrees Of Freedom (DOF) used in the algorithm, or $2N_{\mathrm{DOF}}$. Using this rule, performance within 3 dB of optimal Signal-to-Interference-plus-Noise Ratio (SINR) is obtained. Optimum is defined here as the output SINR of the algorithm given a known interference covariance matrix.

A fully adaptive STAP algorithm uses all available DOF, or MN, where M and N respectively represent the number of pulses within a Coherent Processing Interval (CPI) and the number of antenna elements. The required sample support predicted by Reed's rule is then $2MN$ vectors. Since the number of range bins from which sample support is obtained is typically much less than $2MN$, secondary data support is a problem. Limited data support drives the need for reduced dimension STAP algorithms; reducing N_{DOF} generates a corresponding decrease in required sample support. The goal of these algorithms has been to obtain maximized SINR performance with small N_{DOF} and correspondingly small secondary data support. In achieving this goal, some algorithms have deviated from the SMI class. One interesting approach is the Cross Spectral Metric (CSM) algorithm developed by Goldstein and Reed [5].

Although Goldstein and Reed assume secondary data support greater than MN [6], operation of the algorithm is shown in this report to be experimentally possible for secondary data set sizes below this value. However, operation in this region does result in a singular covariance matrix and algorithm performance correspondingly suffers. The report examines the operation of the CSM algorithm with secondary data set sizes on the order of MN. The results show the algorithm is capable of operating with a singular covariance matrix through an appropriate choice of N_{DOF}. Best performance occurs when N_{DOF} equals the interference subspace dimension. This result is reaffirmed through a mathematical analysis using an eigenbeam model originally used for SMI techniques [2–4]. Furthermore, the analysis introduces a method to mitigate the effects of insufficient sample support on the CSM algorithm when N_{DOF} is chosen inappropriately.

1.1 Notation

Commonly accepted mathematical notation is used throughout the report. Matrices are represented by upper case bold letters, such as $\mathbf{R}$ and $\mathbf{\Lambda}$. Vectors use lower case bold letters, for example $\mathbf{e}$ or $\boldsymbol{\chi}$. The superscript ^{T} and ^{H} operators denote the transpose and Hermitian operators respectively. Vertical bars, $|\cdot|$, represent the absolute value operator. The expected value operator is denoted $\mathcal{E}\{\cdot\}$. The $N \times N$ identity matrix is $\mathbf{I}_N$. Estimated parameters are denoted with a $\hat{}$ above the variable, e.g. λ might be the true eigenvalue and $\hat{\lambda}$ the estimated eigenvalue.

The simulated antenna array consists of N elements arranged linearly with equal spacing. The adaptive processing is performed within a coherent processing interval (CPI) of M pulses. The term noise is defined to include all thermal effects and any other sources of white, uncorrelated noise. Interference is defined to include the effects of all correlated sources. Any targets placed in the data are discrete representations of constant amplitude.

1.2 Report Overview

A portion of the simulation results presented in this report are a result of thesis work [7] conducted by the author while at the Air Force Institute of Technology. The work was supported by Capt Bill Melvin, formerly of Rome Laboratory now known as the Air Force Research Laboratory (AFRL). The purpose of this report is to expand on the results of [7].

The organization of the report is as follows. The Cross Spectral Metric (CSM) algorithm is reviewed and discussed in Section 2.0. The concept of secondary data support for covariance matrix estimation is also briefly reviewed here. Section 3.0 discusses the simulation results. An analysis of these results can be found in Section 4.0. Section 5.0 gives a set of conclusions that can be drawn from this work.

2.0 THE CSM ALGORITHM

The CSM algorithm as derived by Goldstein [5] is a transformation of the direct form STAP problem into a Generalized Sidelobe Canceller (GSC) architecture. A block diagram of the algorithm is shown in Fig. 1. The purpose of this section is not to present the entire algorithm development, but merely to highlight its important features. Although the algorithm is discussed in detail, it is left to the reader to reference [5,6,8] and obtain a thorough understanding of the derivation.

The CSM algorithm, as most algorithms are, is developed entirely for the case of a known covariance matrix $\mathbf{R}$. In practice, the estimated covariance $\hat{\mathbf{R}}$ is substituted for $\mathbf{R}$. No optimality is claimed for the case of estimated covariance. The purpose of this report is to evaluate algorithm performance in the case of estimated covariance.

Figure 1 illustrates a two step process. An estimate d of the desired signal along with any interference and noise is generated in the upper branch. The interference signal estimate $y_{\mathbf{z}}$ in the lower branch is then subtracted from d. Assuming $y_{\mathbf{z}}$ is an accurate estimate of the interference, the problem is then reduced to the standard case of detecting a target in uncorrelated noise.

The incoming data for the range gate of interest l is defined as $\boldsymbol{\chi}$, the space-time snapshot [9]. The range gate dependence is implicit. The incoming snap-shot is always assumed to correspond to the range gate of interest unless an explicit subscript is added. The column vector $\boldsymbol{\chi}$ is the concatenation of the complex radar returns from each of the N antenna elements for M pulses.

The response of the filter in the upper branch of Fig. 1 is maximized in the direction of the desired signal. The transfer function is the normalized spatio-temporal steering vector[1] $\mathbf{s}$, allowing the output of the upper branch to be written as

$$d = \mathbf{s}^H \boldsymbol{\chi}. \tag{1}$$

The lower branch of the block diagram shows a vector $\mathbf{b}$ equal to $\mathbf{B}\boldsymbol{\chi}$, where $\mathbf{B}$ is a blocking matrix defined such that $\mathbf{Bs} = \mathbf{0}$ and is of dimension $(MN-1) \times MN$. The covariance matrix is defined as [9]

$$\mathbf{R} = \mathcal{E}\{\boldsymbol{\chi}\boldsymbol{\chi}^H\}. \tag{2}$$

Using this definition, the covariance matrix for $\mathbf{b}$ is

$$\mathbf{R_b} = \mathcal{E}\{\mathbf{b}\mathbf{b}^H\} = \mathbf{BRB}^H. \tag{3}$$

The eigenvalue decomposition of this matrix is

$$\mathbf{R_b} = \mathbf{U}\boldsymbol{\Lambda}\mathbf{U}^H, \tag{4}$$

[1] See [9] for a derivation of spatial, temporal, and spatio-temporal steering vectors.

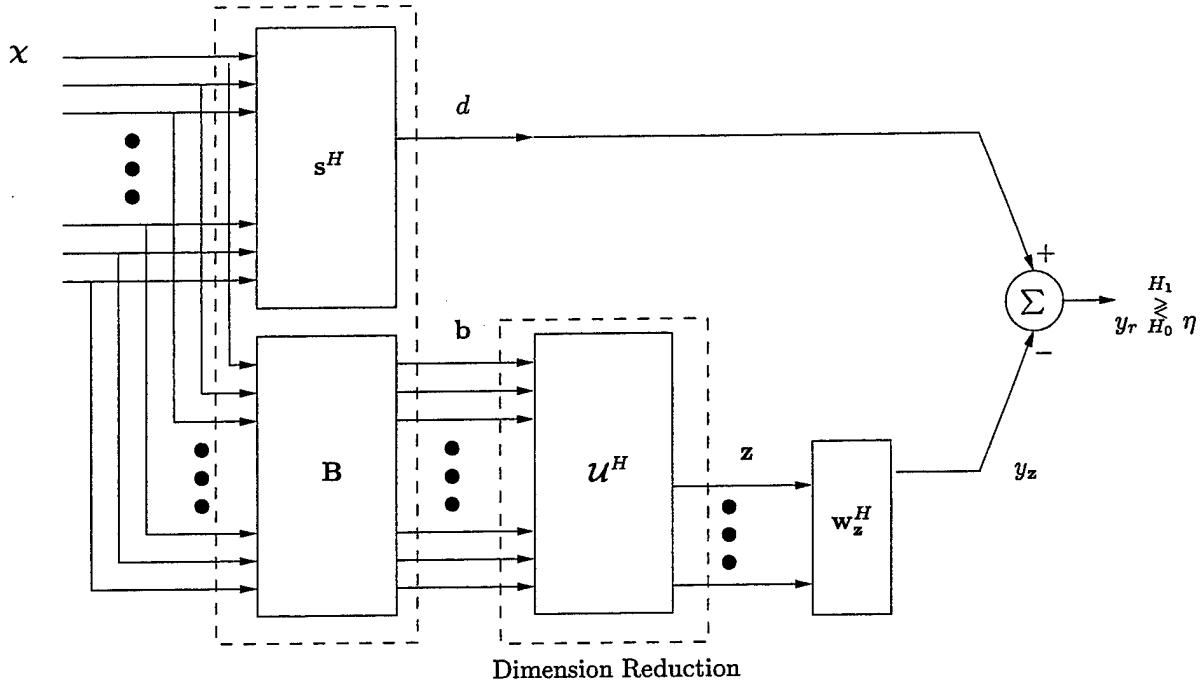

Figure 1: CSM Algorithm Block Diagram.

where $\mathbf{U}$ is the matrix of eigenvectors and $\mathbf{\Lambda}$ is the diagonal matrix of eigenvalues. Mathematically these can be written in terms of the eigenvectors and eigenvalues themselves, i.e.

$$\begin{aligned} \mathbf{U} &= \begin{bmatrix} \nu_1 & \nu_2 & \dots & \nu_{MN-1} \end{bmatrix} \\ \mathbf{\Lambda} &= \operatorname{diag}\left(\lambda_1, \ \lambda_2, \ \dots, \ \lambda_{MN-1}\right) \end{aligned} \tag{5}$$

The dimension of the algorithm is reduced through the $(MN-1)\times N_{\text{DOF}}$ matrix $\mathcal{U}$, where the columns of this matrix are composed of N_{DOF} eigenvectors from the eigenvalue decomposition of $\mathbf{R_b}$. These eigenvectors are chosen according to the Cross Spectral Metric (CSM) [6],

$$\left| \frac{\nu_i^H \mathbf{r_{bd}}}{\sqrt{\lambda_i}} \right|^2, \tag{6}$$

where $\mathbf{r_{bd}}$ is the cross correlation between d and $\mathbf{b}$, or $\mathcal{E}\{\mathbf{b}d^*\} = \mathbf{BR_s}$. Only the N_{DOF} eigenvectors with the largest CSM are included in $\mathcal{U}$, resulting in optimum SINR for this number of DOF. If we assume the columns of $\mathbf{U}$ and $\mathbf{\Lambda}$ are ordered according to the CSM, then the following equations hold:

$$\begin{aligned} \mathcal{U} &= \mathbf{U}(:, 1 : N_{\text{DOF}}) \\ \mathbf{\Lambda}_{N_{\text{DOF}}} &= \operatorname{diag}\left(\lambda_1, \ \lambda_2, \ \dots, \ \lambda_{N_{\text{DOF}}}\right). \end{aligned} \tag{7}$$

MATLAB® notation has been used to express these equations.

Notice that an eigenvalue equal to zero causes the CSM of Eqn. (6) to be undefined. One should note that all SMI techniques are also undefined for a singular covariance matrix since this matrix type is non-invertible. Although unlikely in a real radar environment due to the effects of thermal noise, the sample covariance matrix estimate is singular when operating with sample support less than MN. Non-singularity can be forced by introducing more white noise into the system through the technique of diagonal loading. This technique is discussed in more detail later.

Disregarding the conditioning problem for the moment, the output of the lower branch is easily written as

$$y_z = \mathbf{w}_z^H \mathcal{U}^H \mathbf{B} \boldsymbol{\chi}, \tag{8}$$

where $\mathbf{w}_z$ is the reduced dimension adaptive filter. This filter is given by [5]

$$\mathbf{w}_z = \boldsymbol{\Lambda}_{N_{\mathrm{DOF}}}^{-1} \mathcal{U}^H \mathbf{r}_{\mathbf{b}d}, \tag{9}$$

where $\boldsymbol{\Lambda}_{N_{\mathrm{DOF}}}$ is the diagonal matrix of eigenvalues corresponding to the N_{DOF} eigenvectors used to form $\mathcal{U}$.

The output of the entire reduced dimension algorithm can then be written as

$$y_r \equiv \mathbf{w}^H \boldsymbol{\chi} = d - y_z = (\mathbf{s} - \mathbf{B}^H \mathcal{U} \boldsymbol{\Lambda}_{N_{\mathrm{DOF}}}^{-1} \mathcal{U}^H \mathbf{r}_{\mathbf{b}d})^H \boldsymbol{\chi}. \tag{10}$$

With this form, the maximum output SINR of the algorithm becomes

$$\mathrm{SINR} \equiv \frac{|\mathbf{w}^H \mathbf{v}|^2}{\mathbf{w}^H \mathbf{R} \mathbf{w}} = \frac{\sigma^2 \xi_t \left| \left(\mathbf{s} - \mathbf{B}^H \mathcal{U} \boldsymbol{\Lambda}_{N_{\mathrm{DOF}}}^{-1} \mathcal{U}^H \mathbf{r}_{\mathbf{b}d} \right)^H \mathbf{v} \right|^2}{\left(\mathbf{s} - \mathbf{B}^H \mathcal{U} \boldsymbol{\Lambda}_{N_{\mathrm{DOF}}}^{-1} \mathcal{U}^H \mathbf{r}_{\mathbf{b}d} \right)^H \mathbf{R} \left(\mathbf{s} - \mathbf{B}^H \mathcal{U} \boldsymbol{\Lambda}_{N_{\mathrm{DOF}}}^{-1} \mathcal{U}^H \mathbf{r}_{\mathbf{b}d} \right)}, \tag{11}$$

where σ^2 is the noise power per element, ξ_t is the target SNR per element per pulse, and $\mathbf{v}$ is the un-normalized space-time steering vector. The steering vector is used because we are interested in the maximum output SINR.

It should be noted that in the case of estimated covariance, $\mathbf{R}$ in Eqn. (11) is *not* replaced by $\hat{\mathbf{R}}$. The covariance matrix estimate is substituted in the weight vector, i.e. $\mathcal{U}$ and $\boldsymbol{\Lambda}_{N_{\mathrm{DOF}}}$ become $\hat{\mathcal{U}}$ and $\hat{\boldsymbol{\Lambda}}_{N_{\mathrm{DOF}}}$, each respectively composed of the eigenvectors and eigenvalues of $\hat{\mathbf{R}}_{\mathbf{b}}$.

2.1 Covariance Matrix Estimation

The covariance matrix is not known in a real radar environment and must be estimated from the data available. The matrices $\hat{\mathcal{U}}$ and $\hat{\boldsymbol{\Lambda}}_{N_{\mathrm{DOF}}}$ are then composed from this estimate. The full dimension covariance matrix is estimated through the use of the Maximum Likelihood (ML) estimator

$$\hat{\mathbf{R}}_l = \frac{1}{K} \sum_{i=l-K/2}^{l+K/2} \boldsymbol{\chi}_i \boldsymbol{\chi}_i^H \text{ for } i \neq l, \tag{12}$$

where l is the range gate of interest, K is the number of secondary data vectors to be used in the estimate, and χ_i is the space-time snapshot or data vector corresponding to the i^{th} range gate. As mentioned previously, Reed's rule for SMI techniques states performance within 3 dB of optimal is obtained with $K \approx 2N_{\text{DOF}}$ [1].

2.2 Generating Data for Performance Analysis

Examining the SINR performance of the CSM algorithm with respect to K was done by generating artificial secondary data. Covariance matrices were generated using models found in Jaffer [10], Ward [9], and Roman [11] to include the effects of clutter, noise, and jammers. The artificial secondary data was generated through the use of the Cholesky decomposition of the desired $\mathbf{R}$,

$$\mathbf{R} = \mathbf{Q}^H\mathbf{Q}, \tag{13}$$

as a coloring filter

$$\tilde{\chi} = \mathbf{Q}^H\mathbf{x}, \tag{14}$$

where $\mathbf{x}$ is complex Gaussian with zero mean, unit variance, and white [12]. The definition of the Cholesky decomposition used here is consistent with MATLAB®.

3.0 SAMPLE SUPPORT AND THE CSM ALGORITHM

The simulation results presented here use two different implementations of the covariance matrix models introduced by Jaffer [10] and contained also by Ward [9] in MATLAB® notation. Scenario 1 is the result of an implementation by the author. Scenarios 2 and 3 use the physical model developed by SSC corporation, fully described in an earlier Rome Laboratory report [11].

3.1 Simulation Procedures

Monte Carlo simulations were used to generate the SINR performance results presented in this report. A new set of white, unit variance data as discussed in Section 2.2 was generated for each trial. The number of trials was generally sufficient to keep the ratio of the mean to the standard deviation of the output SINR on the order of 10 dB. However, this ratio could not be kept when the mean SINR dropped too low, as occurs at the dip exhibited by some SINR curves plotted as a function of sample support size K. Optimum SINR is defined here as the algorithm's output SINR using the known covariance matrix with the same N_{DOF}.

The subspace structure of the covariance matrix is characterized by its eigenvalues. For the purposes of this report,

$$\text{eig}(\mathbf{R}) = \text{interference subspace eigenvalues} + \text{noise subspace eigenvalues}, \tag{15}$$

where the noise subspace is characterized by eigenvalues of equal magnitude and the interference subspace is defined to be all others. The number of eigenvalues in the noise subspace is referred to as its dimension. Similarly, the number of eigenvalues within the interference subspace is its dimension.

3.2 Simulation Results

Figure 2 shows the subspace characteristics of interference scenario 1 for the known covariance matrix. Using parameters from [9], the first covariance matrix as described in Table 1 corresponds to a clutter ridge slope β equal to 1. This value produces a sharp transition from the interference subspace to the noise subspace due to the ideal antenna model, zero crab angle, no channel mismatch/errors, etc. These non-ideal factors all serve to blur the transition from interference to noise subspace. The parameters σ^2 and ξ_t have been set to unity for all simulations.

The 18 elements and 18 pulses yield a maximum space-time product of $MN = 324$ DOF. The plot of the CSM shows a clear transition from the interference subspace to the noise subspace after 65 eigenvectors. The number of eigenvalues corresponding to this transition is referred as the interference subspace dimension.

This figure further shows an interesting and valuable feature of the CSM algorithm. The eigenvalues are plotted in the order of descending CSM magnitude. The relationship between the CSM magnitude and

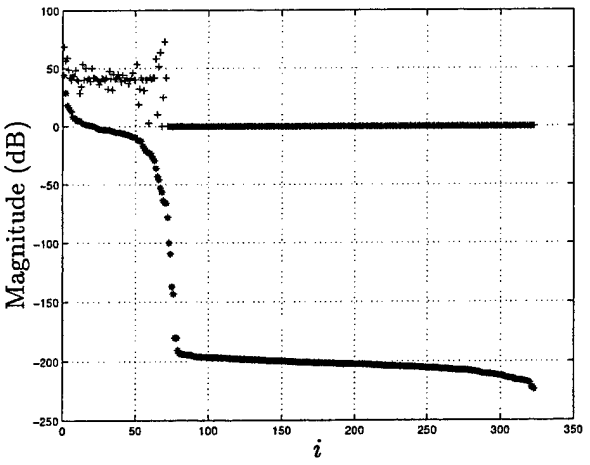

Figure 2: CSM (∗) and corresponding eigenvalue (+) magnitudes for scenario 1 using known covariance.

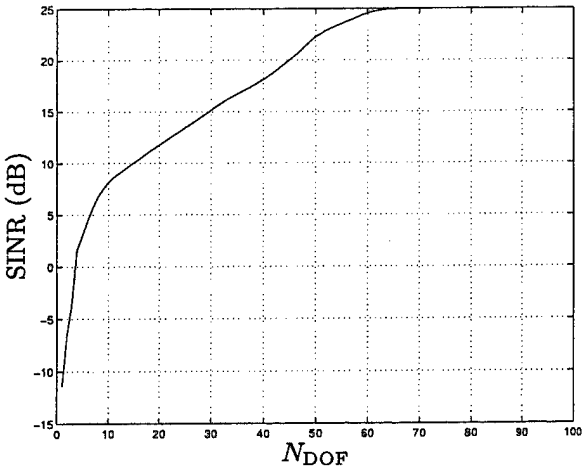

Figure 3: Optimum SINR Curve Versus N_{DOF} for scenario 1.

the eigenvalue magnitude shows the largest eigenvalue is one of the last principle cross spectral components chosen. This is in direct conflict with the method of principle components, which chooses according to the largest eigenvalue.

The first step in determining the impact of varying sample support size K on the CSM algorithm is to find the performance of the algorithm with the known covariance matrix for each scenario. Figure 3 shows the increase in SINR as N_{DOF} increases. The Matched Filter (MF) performance of 25.1 dB SINR, determined from the space-time product MN, is reached with as few as 65 DOF compared to the full dimensional adaptivity of $MN = 324$. SINR roll-off occurs for N_{DOF} below 65 because there are not enough DOF available to counter the interference. The figure provides the optimum SINR, allowing us to calculate the SINR Loss (L_{SINR}) due to insufficient K, i.e. limited sample support, in estimating the covariance matrix for each scenario.

The second scenario uses the covariance matrix generated by the physical model [11] data generation method contained within the Multi-Channel Signal Processing System (MCSPS) designed and constructed by AFRL/SNRT. The space-time product was 32: 8 elements and 4 pulses. The effects of two jammers, clutter, and noise are included. Table 2 gives all of the relevant model parameters. Figure 4 shows large eigenvalues do not necessarily correspond to high CSM values. As a matter of fact, the largest eigenvalue shown in this plot is the 29^{th} highest CSM value, and hence the 29^{th} DOF to be chosen for maximum SINR (when the covariance matrix is known). The trends shown in the figures corresponding to this scenario confirm the result found for the first scenario in that the DOF needed to reach MF performance is typically much less than the space-time product. Figures 4 and 5 illustrate the subspace characteristics of this scenario

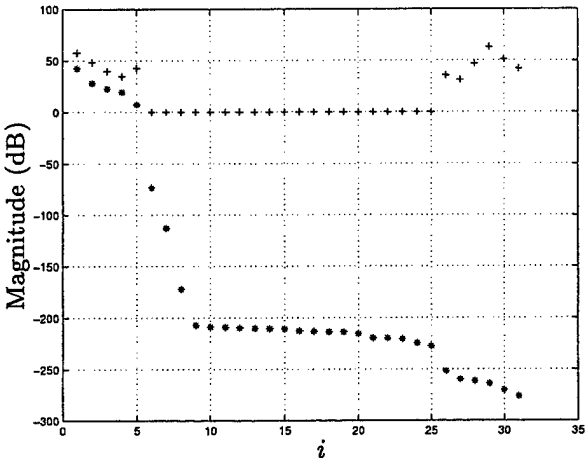

Figure 4: CSM (*) and corresponding eigenvalue (+) magnitudes for scenario 2 using known covariance. The values are plotted in order of descending CSM magnitude.

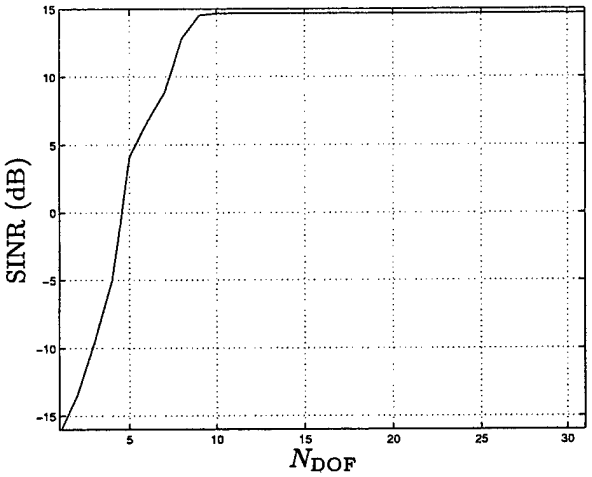

Figure 5: Optimum SINR curve versus N_{DOF} for scenario 2. MF performance is reached with as few as 10 DOF.

(the interference and noise subspace dimensions).

Monte Carlo simulations were used to generate the SINR versus sample support size K curves shown in Fig. 6 through 8 with N_{DOF} as a parameter for interference scenario 1. Figure 6 shows curves with $N_{DOF} \leq 65$ (below the interference subspace dimension). As expected, the SINR performance of each curve improves as K increases. However, none of the curves exhibit the performance within 3 dB of the MF predicted by Reed's rule. In fact, choosing $N_{DOF} < 50$ for this covariance matrix results in the curve never reaching 3 dB of optimal (the MF). Figure 3 provides the reference necessary to determine the SINR loss.

Figure 7 shows the simulation results for scenario 1 but now with N_{DOF} above the dimension of the interference subspace. Again, the performance of the algorithm is optimum with only 65 DOF, but performance drops rapidly with increasing N_{DOF}. Of particular interest is the observation that the decrease in SINR is most dramatic at the sample support size $K = MN = 324$. The results clearly demonstrate the choice of N_{DOF} is critical to the performance of the CSM algorithm in this scenario. If N_{DOF} is chosen larger than the interference subspace dimension, the performance of the algorithm severely suffers when the sample support is close to the space-time product of 324. The performance degradation can be as much as 18 dB. In Section 4.0, we consider the cause of these significant performance losses.

Figure 8 shows similar results for interference scenario 2. As surmised, the maximum SINR performance was obtained with N_{DOF} equal to the interference subspace dimension. Furthermore, the point of maximum SINR loss (the dip) occurs at the new space-time product $MN = 32$. These results confirm the results of scenario 1.

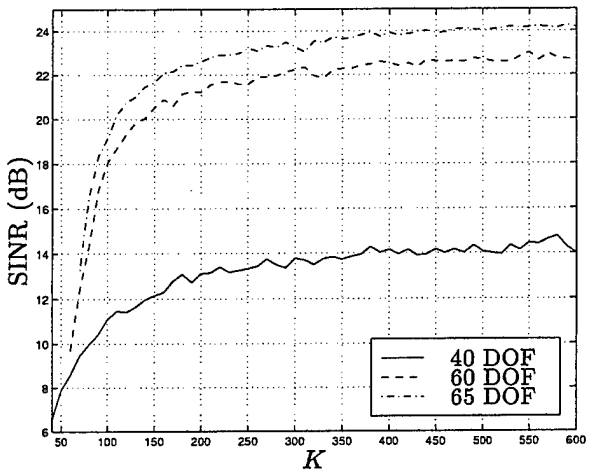

Figure 6: Overlay Of SINR Curves For $N_{\text{DOF}} \leq 65$ For Scenario 1.

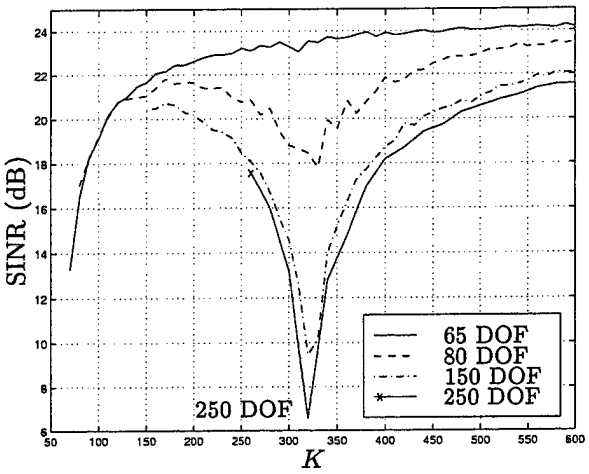

Figure 7: Overlay Of SINR Curves For $N_{\text{DOF}} \geq 65$ For Scenario 1.

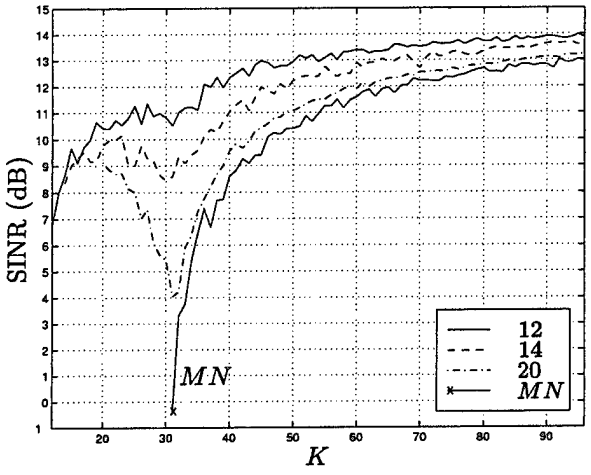

Figure 8: Overlay Of SINR for scenario 2.

4.0 PERFORMANCE ANALYSIS

In Section 3.0, we noted performance is maximized when N_{DOF} is equal to the interference subspace dimension. This result is simply due to the fact that N_{DOF} corresponds to the number of principal cross spectral components of the covariance matrix. Increasing N_{DOF} beyond this value will only add DOF corresponding to the noise subspace. It was previously shown in Figs. 3 and 5 that MF performance was obtained with N_{DOF} equal to the interference subspace dimension when using known covariance.

The more challenging question arising from the research reported here is the cause behind the large drops in SINR occurring when secondary data support size is in the vicinity of the space-time product MN and N_{DOF} is greater than the interference subspace dimension. The answer to this interesting question can be found through an eigenbeam model of covariance matrix estimation error used by [2–4] and is considered next.

4.1 Covariance Matrix Estimation Error

The eigenbeam model expresses the overall antenna pattern in terms of a steering vector pattern minus eigenbeams. The eigenbeams essentially are antenna patterns formed from the eigenvectors of the covariance matrix estimate. We formulate the model for the fully adaptive case using the specification of the standard Sample Matrix Inversion (SMI) algorithm [1, 13],

$$\mathbf{w}_{SMI} = \hat{\mathbf{R}}^{-1}\mathbf{v} \tag{16}$$

where $\hat{\mathbf{R}}$ is the sample covariance matrix obtained from the Maximum Likelihood (ML) estimator and $\mathbf{v}$ is the space-time steering vector.

The eigenbeam model is generated by replacing the sample covariance matrix with its eigenvalue/eigenvector decomposition. We deviate slightly from the notation of the previous section on the CSM algorithm and use $\hat{\mathbf{U}}\hat{\mathbf{\Lambda}}\hat{\mathbf{U}}^H$ to denote the eigenvalue decomposition of $\hat{\mathbf{R}}$, where $\hat{\mathbf{U}}$ denotes the unitary matrix of eigenvectors, $\hat{\nu}_i$ is the i^{th} eigenvector, $\hat{\mathbf{\Lambda}}$ denotes the diagonal matrix of eigenvalues, and $\hat{\lambda}_i$ is the i^{th} eigenvalue. Substituting the decomposition results in

$$\mathbf{w}_{\mathrm{SMI}} = \hat{\mathbf{U}}\hat{\mathbf{\Lambda}}^{-1}\hat{\mathbf{U}}^H\mathbf{v}. \tag{17}$$

We have taken advantage of the inversion property of the unitary eigenvector matrices in the above equation.

We form the eigenbeam model through the following simplifications,

$$
\begin{aligned}
\mathbf{w}_{\mathrm{SMI}} &= \hat{\mathbf{U}}\hat{\mathbf{\Lambda}}^{-1}\hat{\mathbf{U}}^H\mathbf{v} \\
&= \sum_{i=1}^{MN}\frac{1}{\hat{\lambda}_i}\hat{\boldsymbol{\nu}}_i\hat{\boldsymbol{\nu}}_i^H\mathbf{v} \\
&= \frac{1}{\hat{\lambda}_{\min}}\sum_{i=1}^{MN}\left(\frac{\hat{\lambda}_{\min}-\hat{\lambda}_i+\hat{\lambda}_i}{\hat{\lambda}_i}\right)\hat{\boldsymbol{\nu}}_i\hat{\boldsymbol{\nu}}_i^H\mathbf{v} \\
&= \frac{1}{\hat{\lambda}_{\min}}\left[\sum_{i=1}^{MN}\left(\frac{\hat{\lambda}_{\min}-\hat{\lambda}_i}{\hat{\lambda}_i}\right)\hat{\boldsymbol{\nu}}_i\hat{\boldsymbol{\nu}}_i^H\mathbf{v}+\sum_{i=1}^{MN}\frac{\hat{\lambda}_i}{\hat{\lambda}_i}\hat{\boldsymbol{\nu}}_i\hat{\boldsymbol{\nu}}_i^H\mathbf{v}\right] \\
&= \frac{1}{\hat{\lambda}_{\min}}\left[\sum_{i=1}^{MN}\left(\frac{\hat{\lambda}_{\min}-\hat{\lambda}_i}{\hat{\lambda}_i}\right)\hat{\boldsymbol{\nu}}_i\hat{\boldsymbol{\nu}}_i^H\mathbf{v}+\hat{\mathbf{U}}\hat{\mathbf{U}}^H\mathbf{v}\right] \\
&= \frac{1}{\hat{\lambda}_{\min}}\left[\mathbf{v}-\sum_{i=1}^{MN}\underbrace{\left(\frac{\hat{\lambda}_i-\hat{\lambda}_{\min}}{\hat{\lambda}_i}\right)\left(\hat{\boldsymbol{\nu}}_i^H\mathbf{v}\right)}_{\text{Eigenbeam Scaling Factor}}\hat{\boldsymbol{\nu}}_i\right], \qquad (18)
\end{aligned}
$$

(19)

where $\hat{\mathbf{U}}\hat{\mathbf{\Lambda}}\hat{\mathbf{U}}^H = \hat{\mathbf{R}}$.

From this equation, we see the fully adaptive SMI weight vector is composed of a nonadaptive steering vector scaled by the inverse of the smallest eigenvalue minus a weight vector composed of scaled eigenvectors. The pattern described by the eigenvector is termed an eigenbeam. Notice the scale factor on the eigenbeams consists of the projection of the eigenvector onto the steering vector. Therefore, an eigenvector with a large eigenvalue that naturally falls into a steering vector null has little effect on the overall pattern.

The known covariance case is characterized by eigenvalues in the noise subspace being constant and equal to the noise power or variance. Equation (18) illustrates for the *known* covariance case (where $\lambda_i = \lambda_{\min}$ for all $i \in$ the noise subspace) that the eigenbeams associated with the noise have no impact on the overall antenna pattern. The remaining eigenvectors span the interference subspace.

With limited sample support, the covariance matrix and its eigenvalues are incorrectly estimated and $\hat{\lambda}_i \neq \hat{\lambda}_{\min}$ for all $i \in$ the noise subspace. These patterns now detract from the desired features of the ideal antenna pattern. As shown by [2–4], insufficient sample support[2] increases the spread in the eigenvalues associated with the noise subspace thereby increasing the scale factor $\frac{\hat{\lambda}_i-\hat{\lambda}_{\min}}{\hat{\lambda}_i}$. Smaller secondary data support induces greater spread in the eigenvalues and hence these noise eigenbeams have larger impact on $\mathbf{w}_{\mathrm{SMI}}$.

[2]Insufficient sample support refers to any case where $K < \infty$.

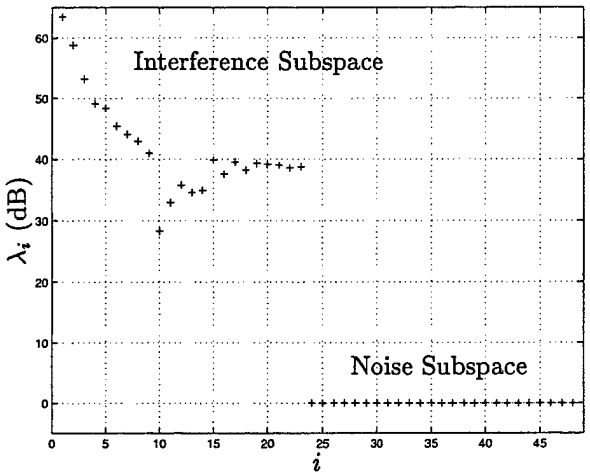

Figure 9: Eigenstructure of the known covariance matrix used for the eigenbeam analysis.

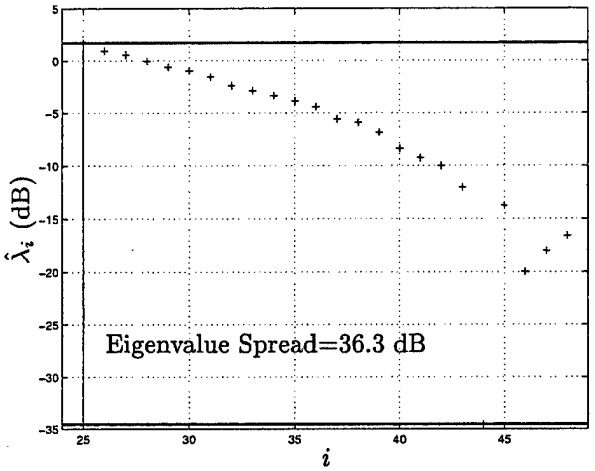

Figure 10: Eigenvalue spread in the noise subspace with MN secondary data vectors, single realization.

Figures 10 through 12 give a graphical interpretation of the eigenvalue spread occurring in the noise subspace with four different secondary data support sizes. The subspace structure of the known covariance matrix used in these examples is shown in Fig. 9.

The relationship between the spread in eigenvalues of the noise subspace and secondary data support K is illustrated in Fig. 13, where the ratio $\frac{\hat{\lambda}_i - \hat{\lambda}_{\min}}{\hat{\lambda}_i}$ is plotted with K as a parameter. The maximum value of unity indicates the eigenbeam has a large impact on the overall antenna pattern. A value of zero indicates the eigenbeam has no impact on $\mathbf{w}_{\mathrm{SMI}}$. Under known covariance, the scale factor is zero for all eigenbeams in the noise subspace.

4.2 Relationship of Estimation Error and CSM

It is of particular interest that the CSM weight vector can be cast in a similar framework. We previously showed in Eqns. 10 and 11 that the weight vector can be written as

$$\mathbf{w} = \mathbf{s} - \mathbf{B}^H \hat{\mathcal{U}} \hat{\Lambda}_{N_{\mathrm{DOF}}}^{-1} \hat{\mathcal{U}}^H \hat{\mathbf{r}}_{\mathbf{bd}}. \tag{20}$$

Through a few minor mathematical manipulations, a form similar to that of the eigenbeam model is obtained:

$$\begin{aligned} \mathbf{w} &= \mathbf{s} - \mathbf{B}^H \sum_{i=1}^{N_{\mathrm{DOF}}} \frac{1}{\hat{\lambda}_i} \hat{\nu}_i \hat{\nu}_i^H \hat{\mathbf{r}}_{\mathbf{bd}} \\ &= \mathbf{s} - \mathbf{B}^H \sum_{i=1}^{N_{\mathrm{DOF}}} \left(\frac{\hat{\lambda}_{\min} - \hat{\lambda}_i + \hat{\lambda}_i}{\hat{\lambda}_{\min} \hat{\lambda}_i} \right) \hat{\nu}_i \hat{\nu}_i^H \hat{\mathbf{r}}_{\mathbf{bd}} \end{aligned} \tag{21}$$

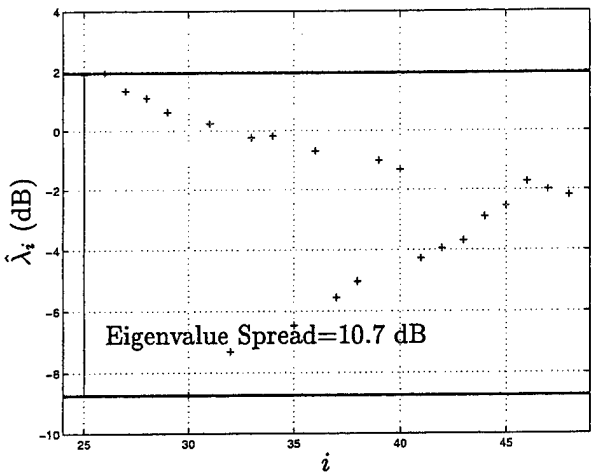

Figure 11: Eigenvalue spread in the noise subspace with $2MN$ secondary data vectors, single realization.

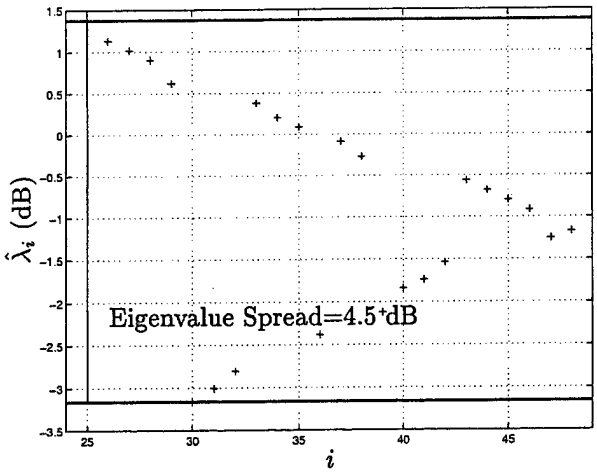

Figure 12: Eigenvalue spread in the noise subspace with $6MN$ secondary data vectors, single realization.

$$\begin{aligned}
\mathbf{w} &= \mathbf{s} - \frac{1}{\hat{\lambda}_{\min}}\mathbf{B}^H \sum_{i=1}^{N_{\mathrm{DOF}}} \left[1 - \left(\frac{\hat{\lambda}_i - \hat{\lambda}_{\min}}{\hat{\lambda}_i}\right)\right] \left(\hat{\boldsymbol{\nu}}_i^H \hat{\mathbf{r}}_{\mathbf{b}d}\right) \hat{\boldsymbol{\nu}}_i \\
&= \mathbf{s} - \frac{1}{\hat{\lambda}_{\min}}\mathbf{B}^H \hat{\mathcal{U}}\hat{\mathcal{U}}^H \hat{\mathbf{r}}_{\mathbf{b}d} + \frac{1}{\hat{\lambda}_{\min}}\mathbf{B}^H \sum_{i=1}^{N_{\mathrm{DOF}}} \left(\frac{\hat{\lambda}_i - \hat{\lambda}_{\min}}{\hat{\lambda}_i}\right) \left(\hat{\boldsymbol{\nu}}_i^H \hat{\mathbf{r}}_{\mathbf{b}d}\right) \hat{\boldsymbol{\nu}}_i \\
&= \frac{1}{\hat{\lambda}_{\min}} \left[\hat{\lambda}_{\min}\mathbf{s} - \mathbf{B}^H \hat{\mathcal{U}}\hat{\mathcal{U}}^H \hat{\mathbf{r}}_{\mathbf{b}d} + \sum_{i=1}^{N_{\mathrm{DOF}}} \left(\frac{\hat{\lambda}_i - \hat{\lambda}_{\min}}{\hat{\lambda}_i}\right) \left(\hat{\boldsymbol{\nu}}_i^H \hat{\mathbf{r}}_{\mathbf{b}d}\right) \mathbf{B}^H \hat{\boldsymbol{\nu}}_i\right]. \qquad (22)
\end{aligned}$$

The notation has changed slightly from the development of the eigenbeam model with respect to the eigenvalue decomposition, reverting back to that used for the development of the CSM algorithm. The summary below assumes the eigenvectors and eigenvalues within the matrices $\mathbf{U}$ and $\boldsymbol{\Lambda}$ are arranged in order of descending CSM magnitude as determined by Eqn. 6.

$$\begin{aligned}
\hat{\mathbf{U}}\hat{\boldsymbol{\Lambda}}\hat{\mathbf{U}}^H &= \mathbf{B}\hat{\mathbf{R}}\mathbf{B}^H = \hat{\mathbf{R}}_{\mathbf{b}} \\
\hat{\mathbf{U}} &= \left[\hat{\boldsymbol{\nu}}_1 \quad \hat{\boldsymbol{\nu}}_2 \quad \ldots \quad \hat{\boldsymbol{\nu}}_{MN-1}\right] \\
\hat{\boldsymbol{\Lambda}} &= \mathrm{diag}\left(\hat{\lambda}_1, \quad \hat{\lambda}_2, \quad \ldots, \quad \hat{\lambda}_{MN-1}\right) \\
\hat{\mathcal{U}} &= \hat{\mathbf{U}}\left(:, 1 : N_{\mathrm{DOF}}\right) \\
\hat{\boldsymbol{\Lambda}}_{N_{\mathrm{DOF}}} &= \hat{\boldsymbol{\Lambda}}\left(1 : N_{\mathrm{DOF}}, 1 : N_{\mathrm{DOF}}\right) \qquad (23)
\end{aligned}$$

Now we can view the CSM algorithm with respect to the three terms of Eqn. 22. The first term is the scaled nonadaptive steering vector, as in the eigenbeam model. The second term represents a projection of the cross correlation vector $\hat{\mathbf{r}}_{\mathbf{b}d}$. Notice this term is unaffected by eigenvalue spread.

The third term is reminiscent of the eigenbeam model. Here the beam/filter is scaled according to its projection on the cross correlation vector, shown by the term $\hat{\nu}_i^H \hat{\mathbf{r}}_{\mathbf{b}d}$. For this reason, we call the term $\mathbf{B}^H \hat{\nu}_i$ a *cross spectral beam.* This cross spectral beam consists of an eigenvector from the interference covariance matrix estimate $\hat{\mathbf{R}}_{\mathbf{b}}$ projected onto the null space of $\mathbf{s}$.

The cross spectral beam is directly affected by eigenvalue spreading due to poor covariance matrix estimation. Under known covariance, the term $\left(\frac{\hat{\lambda}_i - \hat{\lambda}_{\min}}{\hat{\lambda}_i}\right)$ is zero when N_{DOF} is greater than the interference subspace dimension and contains eigenvector/eigenvalue pairs from the noise subspace. We have already shown the scale factor is near maximum, or unity, when sample support size K is on the order of MN. Therefore, this term contributes a large distortion to the overall adaptive pattern.

Allowing K to fall below MN results in an artificial suppression of the eigenvalue spread due to computational limitations. By definition, the number of non-zero eigenvalues is the rank of a matrix. When $K < MN$, the rank of the covariance matrix is K and there exist $MN - K$ zero eigenvalues. Therefore, there is no spreading and these beams should have no impact on the overall pattern. However, when these eigenvalues are calculated from the covariance matrix estimate, they are not set equal to zero due to the limitations of the computer. These beams still impact the overall antenna pattern but with an artificially suppressed scale factor. This suppression reduces the impact of the cross spectral beams resulting in an increase in output SINR. These observations agree well with the SINR dip results reported in the previous section, where we noted the dip only occurs when N_{DOF} is greater than the dimension of the interference subspace and sample support size K is on the order of MN.

From this analysis, we conclude the underlying cause of the SINR dip observed in Figs. 7 and 8 is insufficient secondary data support. We give further support for this conclusion in the next section through a discussion of diagonal loading. Diagonal loading the covariance matrix estimate reduces the eigenvalue spread in the noise subspace. As we show next, the introduction of diagonal loading mitigates the SINR performance drop.

4.3 Diagonal Loading

The effects of insufficient sample support, as illustrated by the scale factor plot of Fig. 13, can be alleviated through the technique of diagonal loading. This technique is equivalent to adding white noise to the covariance matrix,

$$\hat{\mathbf{R}}_{\mathrm{DL}} = \hat{\mathbf{R}} + \kappa^2 \mathbf{I}_{\mathrm{MN}}. \tag{24}$$

The factor κ^2 is referred to as the diagonal load factor. The squaring is used primarily to emphasize its role as additive white noise. With this convention, κ^2 can be viewed as the variance or noise power added to the

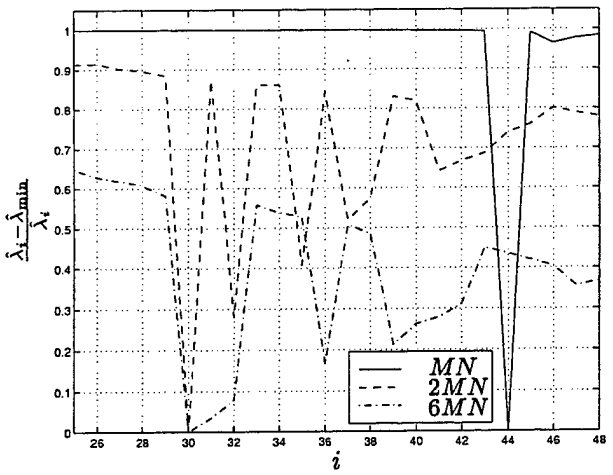

Figure 13: Relationship of the scale factor in Eqn. (18) to sample support for eigenbeams occupying the noise subspace for the eigenbeam analysis example. Plot based on a single realization of $\hat{\mathbf{R}}$.

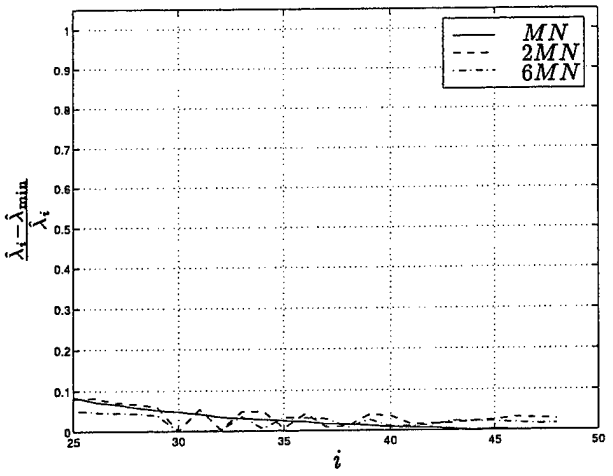

Figure 14: Relationship of the scale factor in Eqn. (18) to sample support for eigenbeams occupying the noise subspace when using diagonal loading with $\kappa^2 = 16$. Plot based on a single realization of $\hat{\mathbf{R}}$.

system.

The technique of diagonal loading works because it reduces the eigenvalue spread. Examining the eigenvalue decomposition of the covariance matrix shows how the technique directly impacts the eigenvalues. Begin by decomposing the covariance matrix estimate with an eigenvalue/eigenvector decomposition,

$$\hat{\mathbf{R}} = \mathbf{U}\mathbf{\Lambda}\mathbf{U}^H. \tag{25}$$

Substitute this alternate expression for $\hat{\mathbf{R}}$ into Eqn. (24) and take advantage of the unitary property of the eigenvector matrix,

$$\begin{aligned} \hat{\mathbf{R}}_{\mathrm{DL}} &= \mathbf{U}\mathbf{\Lambda}\mathbf{U}^H + \kappa^2\mathbf{I}_{\mathrm{MN}} \\ &= \mathbf{U}\mathbf{\Lambda}\mathbf{U}^H + \mathbf{U}\kappa^2\mathbf{I}_{\mathrm{MN}}\mathbf{U}^H \\ &= \mathbf{U}\left(\mathbf{\Lambda} + \kappa^2\mathbf{I}_{\mathrm{MN}}\right)\mathbf{U}^H. \end{aligned} \tag{26}$$

The above expression shows the diagonal load parameter directly adds to the eigenvalues and has no impact on the eigenvectors. Therefore, by using this technique, we can control the eigenvalue spread and hence control the impact of the noise subspace eigenbeams.

Figure 14 shows the impact of diagonal loading on the scale factor with $\kappa^2 = 16$ for the same scenario and data realizations as in Fig. 13. The large diagonal load factor is possible because of the large separation between interference and noise eigenvalues in this example. The resulting drop in scale factor magnitude indicates the eigenbeams have much less impact on the overall antenna pattern.

There are significant trade-offs in the technique. Diagonal loading performs very well when there is a distinct noise subspace that is well separated from the interference subspace, such as the ones shown in Figs. 2, 4, and 9. In these cases, a large diagonal load can be used to decrease the eigenvalue spread in the noise subspace with little impact on the spread in the interference subspace (due to the large eigenvalues of the interference subspace as compared to the noise subspace). However, a gradual transition between the subspaces means κ^2 is significant when compared to eigenvalues of the interference subspace. Any diagonal loading can negatively impact the desired pattern features by modifying the contributions from the interference eigenbeams.

Figure 15 shows the impact of diagonal loading the covariance matrix estimate with $\kappa^2 = 16$ for scenario 2. This figure is the diagonal loaded counterpart to Fig. 8. As we expected from the above analysis, the algorithm's performance is significantly improved. The drop in SINR performance evident with no diagonal loading has been eliminated. Furthermore, the overall SINR performance of the fully adaptive case is improved for small values of K. The results are dramatic because of the choice of scenario (very distinct difference between interference and noise subspaces).

A third scenario was created to further explore the impact of diagonal loading on the CSM algorithm. We previously hypothesized the diagonal loading technique would break down when the noise subspace was no longer distinctly separated from the interference subspace. This scenario creates this condition through the introduction of a 7 deg crab angle. This step alone was insufficient to obtain the desired eigenstructure, therefore a total of 6 jammers were also included. Figure 16 shows the scenario structure in terms of the eigenvalues and CSM. Table 3 shows the parameters used to build the covariance matrix using the physical model.

The impact of diagonal loading this covariance scenario is shown in Fig. 17. The first point of interest is the absence of the dip corresponding to the space-time product exhibited by the earlier plots. As surmised earlier and now shown by example, the dip is an artifact of estimation in the noise subspace with insufficient sample support. When the noise subspace is mitigated, the dip disappears. Optimum SINR only reached 8.16 dB due to the large number of jammers in the scenario. The poor SINR performance of the reduced dimension curves is due to the large interference subspace, more DOF are required to mitigate the interference environment.

The second point to be made with these plots is the loss in SINR due to the diagonal loading. The diagonal loading does show a significant improvement in SINR when N_{DOF} is equal to the fully adaptive case for small secondary data support near the space-time product. However, as secondary data support increases there is a small loss in SINR due to the diagonal loading as K increases. The diagonal load gives improvement for K near the space-time product of MN. This occurs because the diagonal load is now

masking important features of the scenario instead of just noise. This fact is very difficult to ascertain from this figure. The loss is noticeable when $K = 95$ and $N_{\mathrm{DOF}} = MN$. A larger κ^2 value would have exaggerated this SINR loss.

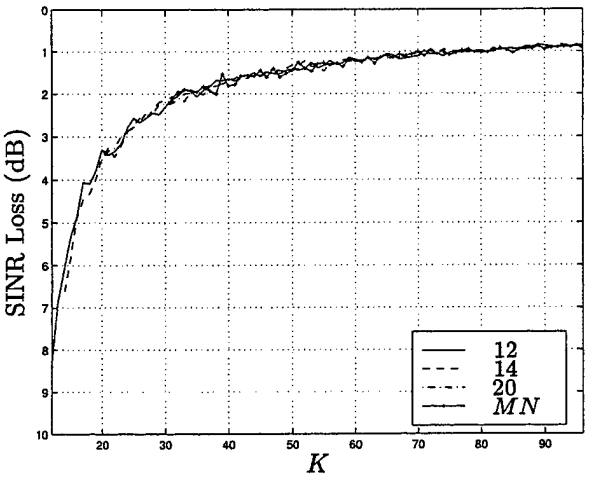

Figure 15: Impact of diagonal loading the covariance matrix estimate on CSM algorithm performance with small data set sizes for scenario 2. The legend refers to the DOF used in the experiment.

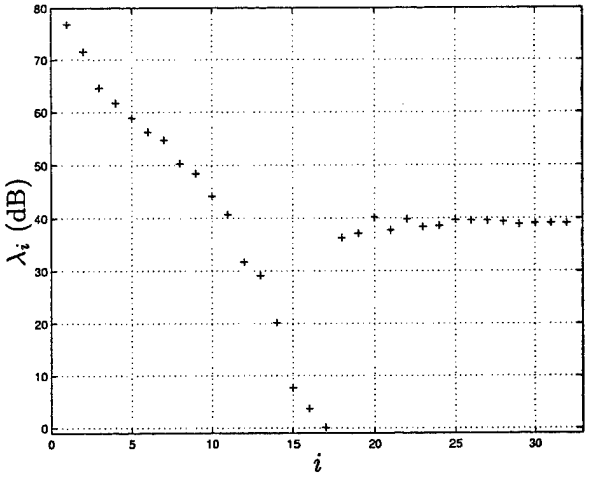

Figure 16: The subspace structure for scenario 3 shown with eigenvalues. This scenario purposely has only one eigenvalue in the noise subspace ($i = 17$).

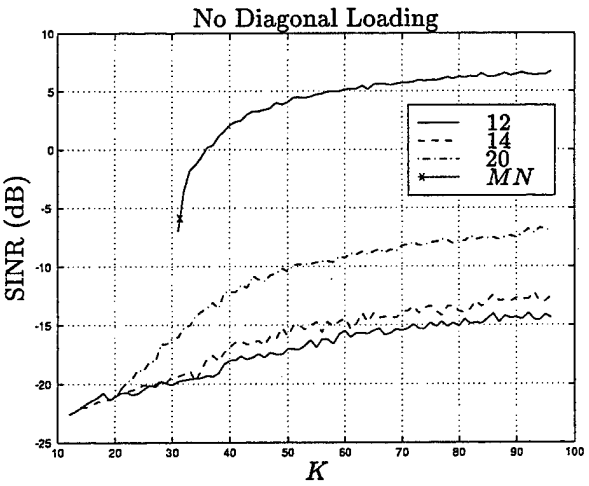

(a)

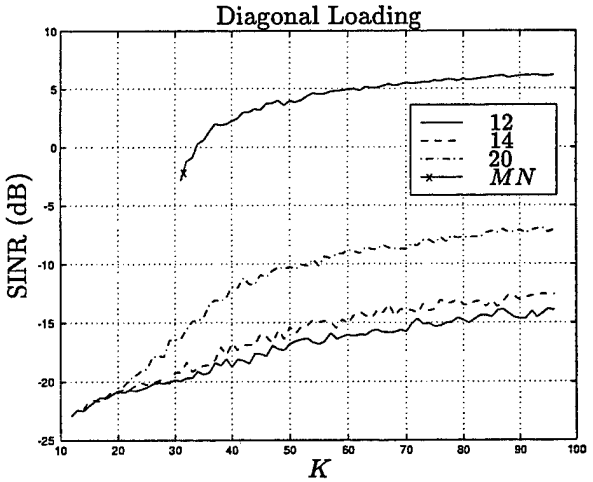

(b)

Figure 17: Impact of diagonal loading the covariance matrix estimate on CSM algorithm performance with small data set sizes for scenario 3 with $MN = 32$. The legend refers to the DOF used in the experiment. The diagonal loading factor κ^2 was 16. As expected, no dip in SINR is evident in (a) because the eigenvalue spread has been minimized due to the scenario parameters.

5.0 CONCLUSIONS

The eigenvalue/eigenvector decomposition of the estimated disturbance covariance matrix $\hat{\mathbf{R}}_{\mathbf{b}}$ in the CSM algorithm brought into question the validity of Reed's rule regarding the required sample support. A Monte Carlo analysis was performed to demonstrate, first, that Reed's rule does hold when the CSM algorithm is fully adaptive and, second, the rule does not hold when $N_{\mathrm{DOF}} < MN$ (the partially adaptive case). This conclusion follows intuition because the fully adaptive CSM algorithm is equivalent to the fully adaptive SMI algorithm.

The performance of the CSM algorithm with estimated covariance is maximized when N_{DOF} is chosen equal to the interference subspace dimension. This result follows expectations because it amounts to choosing all of the principle cross spectral components. Furthermore, the experimental SINR performance of the algorithms as N_{DOF} approaches MN showed the expected convergence to the fully adaptive case. However, an unexpected result was the susceptibility of this algorithm to poor estimation in the noise subspace. This weakness was manifested in the large SINR dip occurring at sample support sizes near the space-time product MN.

In an effort to determine the cause of the SINR dip, an exploration of the eigenbeam model [2–4] was presented. The CSM algorithm was shown mathematically to contain many of the characteristics of the eigenbeam model. One of the most important characteristics is the impact of eigenvalue spread in the noise subspace. In particular, the direct relationship between eigenvalue spread and sample support was shown to perturb the overall weight vector.

Of the scenarios chosen for the analysis, the first two illustrated a severe drop in SINR occurring at secondary data support sizes equal to the space-time product MN. The third scenario did not exhibit the drop because the interference subspace was purposely forced to consume the entire subspace structure of the covariance matrix, thereby increasing the value of $\hat{\lambda}_{\mathrm{min}}$ and decreasing eigenvalue spread. In this situation, the overall antenna pattern does not experience significant degradation because the eigenvalue spread is mitigated through the scenario itself.

Diagonal loading was used to eliminate the SINR performance drop for the first two scenarios. The trade-offs of diagonal loading for different scenario types were briefly explored. In particular, it was shown that diagonal loading is not a cure all technique. The choice of the diagonal load factor is scenario dependent and crucial to avoid impacting the desired portions of the antenna pattern. Diagonal loading does represent a powerful tool that can be used to gain significant improvement in SINR performance.

Parameter	*Value*	
Elements (M)	18	
Pulses (N)	18	
Normalized Element Spacing	0.5	
Mainbeam Transmit Az	0	deg
Peak Transmit Power	200	kW
Uncompressed Pulse Duration	200	μsec
Pulse Repetition Frequency	300	Hz
Carrier Frequency	1240	MHz
Receiver Bandwidth	4	MHz
Transmit Pattern Gain	22	dB
Receive Pattern Gain	10	dB
Receive Element Backlobe Attenuation	30	dB
System Noise Figure	10	dB
System Loss	4	dB
Thermal Noise Power	1	W
Transmit Array Pattern	Uniform	
Platform Altitude	9	km
Platform Velocity	50	m/s
Range to Clutter Ring	80	km
Number of Clutter Ring Patches	361	
Platform Crab Angle	0	deg
Target Radial Velocity	33.33	m/s
Target Normalized Doppler ($\bar{\omega}_t$)	0.5	
Target Azimuth (θ_t)	0	deg
Target Elevation	0	deg
Number of Jammers	2	
Jammer Azimuths	$[\ -40 \quad 25\ ]$	deg
Jammer Elevations	zeros$(1,2)$	deg
Jammer Powers	$1000 * \text{ones}(2,1)$	W
Jammer Ranges	$[\ 370 \quad 370\ ]$	km
Jammer-to-Noise Ratios	$[\ 27.79 \quad 29.25\ ]$	dB

Table 1: Parameters for scenario 1. The physical model was used to generate covariance matrices [11]. This scenario is the result of the author's implementation.

Parameter	*Value*	
Elements (M)	8	
Pulses (N)	4	
Normalized Element Spacing	0.5	
Mainbeam Transmit Az	0	deg
Peak Transmit Power	200	kW
Uncompressed Pulse Duration	200	μsec
Pulse Repetition Frequency	300	Hz
Carrier Frequency	450	MHz
Receiver Bandwidth	4	MHz
Transmit Pattern Gain	22	dB
Receive Pattern Gain	10	dB
Receive Element Backlobe Attenuation	30	dB
System Noise Figure	10	dB
System Loss	4	dB
Thermal Noise Power	1	W
Transmit Array Pattern	Uniform	
Platform Altitude	9	km
Platform Velocity	50	m/s
Range to Clutter Ring	130	km
Number of Clutter Ring Patches	361	
Platform Crab Angle	0	deg
Target Radial Velocity	33.33	m/s
Target Normalized Doppler ($\bar{\omega}_t$)	0.5	
Target Azimuth (θ_t)	0	deg
Target Elevation	0	deg
Number of Jammers	0	
Jammer Azimuths	NA	deg
Jammer Elevations	NA	deg
Jammer Powers	NA	W

Table 2: Parameters for scenario 2. The physical model was used to generate covariance matrices [11]. The covariance matrix was generated using the Multi-Channel Signal Processing System (MCSPS) developed by AFRL/SNRT.

Parameter	*Value*	
Elements (M)	8	
Pulses (N)	4	
Normalized Element Spacing	0.5	
Mainbeam Transmit Az	0	deg
Peak Transmit Power	400	kW
Uncompressed Pulse Duration	400	μsec
Pulse Repetition Frequency	600	Hz
Carrier Frequency	450	MHz
Receiver Bandwidth	4	MHz
Transmit Pattern Gain	22	dB
Receive Pattern Gain	10	dB
Receive Element Backlobe Attenuation	30	dB
System Noise Figure	10	dB
System Loss	4	dB
Thermal Noise Power	1	W
Transmit Array Pattern	Uniform	
Platform Altitude	9	km
Platform Velocity	50	m/s
Range to Clutter Ring	80	km
Number of Clutter Ring Patches	361	
Platform Crab Angle	7	deg
Target Radial Velocity	33.33	m/s
Target Normalized Doppler ($\bar{\omega}_t$)	0.33	
Target Azimuth (θ_t)	0	deg
Target Elevation	0	deg
Number of Jammers	6	
Jammer Azimuths	$[\ -25 \quad 40 \quad -10 \quad -65 \quad 65 \quad 25\ ]$	deg
Jammer Elevations	zeros$(1,6)$	deg
Jammer Powers	$1000 * \text{ones}(6,1)$	W

Table 3: Parameters for scenario 3. The physical model was used to generate covariance matrices [11]. This covariance matrix was generated using the Multi-Channel Signal Processing System (MCSPS) developed by AFRL/SNRT.

References

[1] I. S. Reed, J. Mallett, and L. Brennan, "Rapid convergence rate in adaptive arrays," *IEEE Transactions on Aerospace and Electronic Systems*, vol. AES-10, No. 6, pp. 853–863, Nov. 1974.

[2] W. F. Gabriel, "Using spectral estimation techniques in adaptive array systems," in *Phased Arrays 1985 Symposium-Proceedings*, no. RADC-TR-85-171, (Rome Air Development Center (RADC), Air Force Systems Command, Griffiss Air Force Base, NY 13441-5700), pp. 109–131, Aug. 1985.

[3] W. F. Gabriel, "Using spectral estimation techniques in adaptive processing antenna systems," *IEEE Transactions on Antennas and Propagation*, vol. AP-34, pp. 291–300, Mar. 1986.

[4] B. D. Carlson, "Covariance matrix estimation errors and diagonal loading in adaptive arrays," *IEEE Transactions on Aerospace and Electronic Systems*, vol. 24, pp. 397–401, July 1988.

[5] J. Goldstein and I. Reed, "Subspace selection for partially adaptive sensor array processing," *IEEE Transactions on Aerospace and Electronic Systems*, vol. 33, No. 2, pp. 539–544, Apr. 1997.

[6] J. S. Goldstein and I. S. Reed, "Theory of partially adaptive radar," *IEEE Transactions on Aerospace and Electronic Systems*, vol. 33, No. 4, pp. 1309–1325, Oct. 1997.

[7] T. Hale, "Secondary data support and non-homogeneities in space-time adaptive processing," Master's thesis, Graduate School of Engineering, Air Force Institute of Technology (AETC), 1997.

[8] J. S. Goldstein and I. S. Reed, "A tutorial on space-time adaptive processing," *IEEE National Radar Conference*, May 1997.

[9] J. Ward, "Space-time adaptive processing for airborne radar," Contract F19628-95-C-0002, Lincoln Laboratory, Massachusetts Institute of Technology, Lexington, Massachusetts, Dec. 1994.

* [10] A. Jaffer, M. Baker, W. Ballance, and J. Staub, "Adaptive space-time processing techniques for airborne radars," Contract F30602-89-D-0028, Hughes Aircraft Company, Fullerton, CA 92634, July 1991.

[11] J. R. Roman and D. W. Davis, "Multichannel system identification and detection using output data techniques," Contract C-F30602-93-C-0193, RL-TR-97-5, Rome Laboratory/OCSM, 26 Electronic Parkway, Rome, NY 13441-4514, May 1997. Volume II of II.

[12] S. M. Kay, *Fundamentals of Statistical Signal Processing, Estimation Theory.* Upper Saddle River, NJ 07458: Prentice-Hall, 1993.

[13] L. Brennan and I. Reed, "Theory of adaptive radar," *IEEE Transactions on Aerospace and Electronic Systems*, vol. AES-9, No. 2, pp. 237–252, Mar. 1973.